ParCFD2024
35th International Conference on Parallel Computational Fluid Dynamics
Sep. 02-04, 2024, Bonn, Germany

Domain Decomposition Method for Equivalent Sources Method in Aeroacoustic

Naima Débit[a], Roland Denis[a], Benoit Fabrege[a] and Damien Tromeur-Dervout[a,*]

[a] *Université Claude Bernard Lyon 1, CNRS, Institut Camille Jordan, UMR5208, 69100 Villeurbanne, France*

ARTICLE INFO[†]

Keywords:
Parallel Methodology;
Domain Decomposition Method;
Equivalent Source Method;
Model Order Reduction

ABSTRACT

This contribution focuses on a Schwarz-type domain decomposition method for solving an ill-conditioned dense linear problem overdetermined with complex coefficients arising from the inverse problem of determining, by the method of equivalent sources, the aeroacoustic noise generated by a fluid on the surface of a body.

1. Introduction

The Equivalent Source Method (ESM) aiming at the simulation of realistic Frequency Response Functions (FRF) substitutes the acoustic behavior of a radiating object by a set of N_s acoustic monopoles q calibrated with respect to the boundary condition v on its skin. The method is a meshless approach so that it is easy and simple to implement, and it does not have a numerical singularity problem that occurs in the boundary element method [1]. Such a method allows to perform 3D Conventional Beamforming (CBF) with FRF considering the acoustic environment and the influence structure [2, 3].

The set ω of N boundary points at position $(r_j)_{j\leq N}$ on the object skin and the set Ω of N_s equivalent sources at the position $(r_l)_{l\leq N_s}$, allow to build the matrix coefficients of the transfer function for the wave number k between the equivalent sources and the normal velocity, with θ_{jl} the angle of $r_j - r_l$ and the normal to the object skin at r_j, as

$$A_{jl} = \frac{e^{ik||r_j-r_l||_2}}{4\pi||r_j-r_l||_2^2}(1-ik||r_j-r_l||_2)\cos(\theta_{jl}).$$

This contribution presents a Schwarz-type domain decomposition method for solving this overdetermined, dense and ill-conditioned linear system $Aq = v, A \in \mathbb{C}^{N\times N_s}$. The ESM suffers from the numerical instability that is associated with the ill-conditioned matrix A due to the random distribution of equivalent sources [1, 4].

[†] This paper is part of the ParCFD 2024 Proceedings. A recording of the presentation is available on YouTube. The DOI of this document is 10.34734/FZJ-2025-02516 and of the Proceedings 10.34734/FZJ-2025-02175.

*Corresponding author
naima.debit@univ-lyon1.fr (N. Débit);
roland.denis@math.univ-lyon1.fr (R. Denis);
benoit.fabrege@math.univ-lyon1.fr (B. Fabrege);
damien.tromeur-dervout@univ-lyon1.fr (D. Tromeur-Dervout)
ORCID(s): 0000-0001-6761-5470 (N. Débit); 0000-0002-9276-4512 (R. Denis); - (B. Fabrege); 0000-0002-0118-8100 (D. Tromeur-Dervout)

2. Schwarz-type domain decomposition

The Restricted Additive Schwarz domain decomposition method (DDM), see, e.g., [5] and references therein, with a well-posed linear system has convergence/divergence properties allowing its acceleration of the convergence to the correct solution. Here, difficulties arise because the matrix A is a complex non-square matrix, and it is also a dense matrix, where each source contributes to each control point. Consequently, there is no natural interface to control the splitting of the domain(s).

2.1. Schwarz DDM based on the geometrical splitting

To define the DDM partitioning in m pairs $\{(\omega_l, \Omega_l), l = 1, \dots, m\}$ of subdomains overlapping or not, ω and Ω are split as follows: from a mesh of the surface (where the vertices are the control points), and the equivalent sources within the object, we divide the surface in m partitions using the METIS graph partitioning library, based on the vertices adjacency. Then, we assign to each equivalent source the rank of the nearest control point using a K-D tree.

With the given partitioning, we iteratively solve Eq. (1), where A_{ij} represents the block of the original matrix with respect to the partition renumbering and A_{ii}^{+} is the pseudo inverse of the block A_{ii}, in order to update the iterated solution $x_i^{(k+1)}$ with respect to the iterated solution $x^{(k)}$, i.e.,

$$x_i^{(k+1)} = A_{ii}^{+}\left(b_i - \sum_{1=j\neq i}^{m} A_{ij}x_j^{(k)}\right). \quad (1)$$

Nevertheless, the resulting method is a divergent method (even with the addition of a relaxation parameter where it converges before diverging). The pure linear convergence/divergence is lost due to ill-conditioning and solving of Eq. (1) in the least squares sense. Moreover, the singular value decomposition (SVD) of the A_{ij} blocks shows that some of them contribute strongly to the b_i RHS, see Fig. 2a.

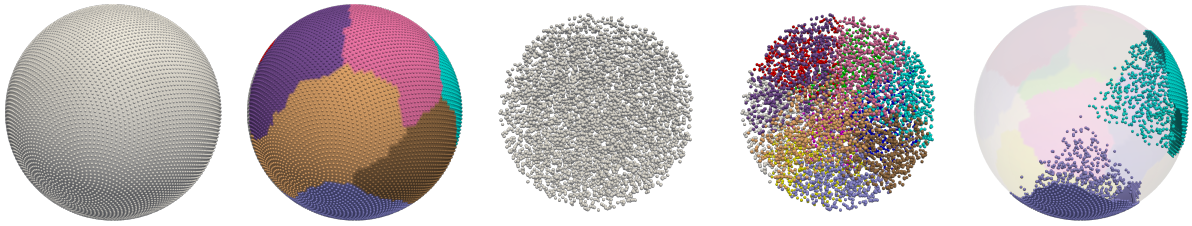

Figure 1: From the left to the right: surface ω of control points, non-overlapping partition of ω, volume Ω of randomly distributed equivalent sources, partitioning of the volume with respect to the ω partitioning, example of two resulting subdomain pairs (ω_l, Ω_l).

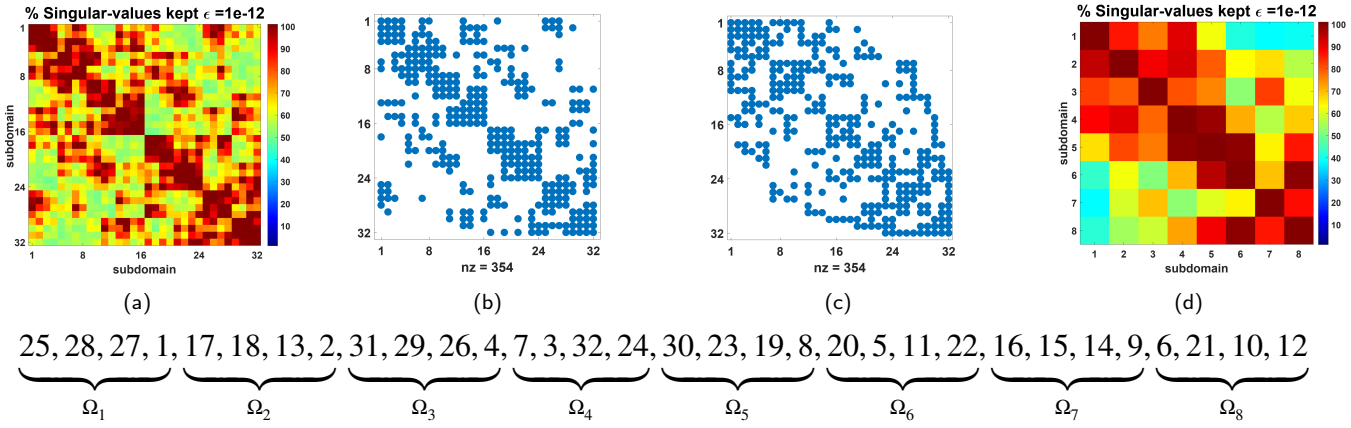

Figure 2: Numerical criterion splitting process starting from a geometrical partitioning of 32 partitions to obtain a partitioning with 8 partitions.

2.2. Numerical criterion splitting

Figure 2 shows the partitioning based on a numerical criterion. The idea is to take into account the factor $1/r^2$ in the matrix coefficients. Starting from the geometrical partitioning with a greater number of partitions than the expected final number, we compute the SVD of each block, see Fig. 2a, and define the threshold criterion τ as % of the number of singular values greater than a given ϵ (here $\epsilon = 10^{-12}$). It produces an adjacency matrix (b) of blocks satisfying this criterion, see Fig. 2b. We reduce the profile of this adjacency matrix with the reverse Cuthill MacKnee's algorithm, see Fig. 2c. We then gather the adjacent blocks to define the new partitioning, see Fig. 2d.

2.3. Projected Schwarz algorithm to handle over-determined systems

We use the SVD $U_{ji}S_{ji}V_{ji}^* = A_{ji}$ of each block A_{ji} of the new partitioning to define a projected Schwarz algorithm where the right hand side of the local problem is projected on the left singular vectors associated with singular values greater than ϵ of each block acting on the components of $x_i^{(k+1)}$. This leads to solving a compressed system with a ξ percentage of the N rows of the original one. The solution of the i^{th} partition reads

$$\bar{A}_i x_i^{(k+1)} = \mathbb{U}_i^* \left(b - \tilde{A}\right), \tag{2}$$

with

$$\bar{A}_i = \begin{pmatrix} S_{1i}V_{1i}^* \\ \vdots \\ S_{mi}V_{mi}^* \end{pmatrix}, \quad \mathbb{U}_i^* = \begin{pmatrix} U_{1i}^* & & \\ & \ddots & \\ & & U_{mi}^* \end{pmatrix}, \quad b = \begin{pmatrix} b_1 \\ \vdots \\ b_m \end{pmatrix}$$

and

$$\tilde{A} = A\left(x_1^{(k)}, \ldots, x_{i-1}^{(k)}, 0_i, x_{i+1}^{(k)}, \ldots, x_m^{(k)}\right)^t = \begin{pmatrix} A_{11} \cdots A_{1i-1} & A_{1i+1} \cdots A_{1m} \\ \vdots & \vdots \\ A_{m1} \cdots A_{mi-1} & A_{mi+1} \cdots A_{mm} \end{pmatrix} \begin{pmatrix} x_1^{(k)} \\ \vdots \\ x_{i-1}^{(k)} \\ x_{i+1}^{(k)} \\ \vdots \\ x_m^{(k)} \end{pmatrix}.$$

This compressed local system Eq. (2) is solved by SVD with a better conditioning than the full system with about 10 orders

$N_s = 3{,}200$	1	2	3	4	5	6	7	8
1	**390**	352	313	360	252	166	151	159
2	369	**409**	365	364	319	257	264	224
3	323	325	**408**	316	302	211	327	249
4	347	373	321	**394**	393	290	223	275
5	258	335	314	393	**401**	402	254	344
6	171	254	212	276	381	**404**	273	398
7	151	244	285	206	243	259	**395**	351
8	166	224	240	284	360	400	340	**399**
$N = 6{,}400$	**2,175**	**2,516**	**2,458**	**2,593**	**2,651**	**2,389**	**2,227**	**2,399**
$\xi = 100\%$	34%	39%	38%	41%	41%	37%	35%	37%

Table 1
Size of system $\bar{A}_i$ for the sphere problem, $N_s = 3{,}200, N = 6{,}400, k = 400\,\text{Hz}, \epsilon = 10^{-12}, \tau = 0.8$.

$log_{10}(cond(A))$	$log_{10}(cond(\bar{A}_i))$							
	1	2	3	4	5	6	7	8
18.87	9.37	7.98	9.12	7.65	7.86	8.71	9.02	7.88

Table 2
The quantity $log_{10}(cond(\bar{A}_i))$ for the sphere problem, $N_s = 3{,}200, N = 6{,}400, k = 400\,\text{Hz}, \epsilon = 10^{-12}, \tau = 0.8$.

of magnitude, see Tab. 2. Recalling the SVD complexity of $O(N\,N_s\,\min(N, N_s))$ for $A \in \mathbb{C}^{N\times N_s}$, we have for the SVD computing of $\bar{A}_i$ a theoretical numerical speed-up of m/ξ and m^2/ξ if it is done in parallel over m processes.

3. First results and conclusion

We consider a monopole scattered by a rigid sphere problem as described in [2].

Table 1 gives the size of the $\bar{A}_i$ system after compression, for the sphere problem with: $N_s = 3{,}200, N = 6{,}400, k = 400\,\text{Hz}, \epsilon = 10^{-12}, \tau = 0.8$ and the last row represents the ξ percentage of compression of $\bar{A}_i$ with respect to the original size of $N = 6{,}400$. The value of ξ is between 34% and 41%. Table 1 also gives details of the size of the compressed system resulting from the A_{ji} block. For example, A_{81} has 399 rows and the compressed block $S_{81}V_{81}^*$ has 166 rows.

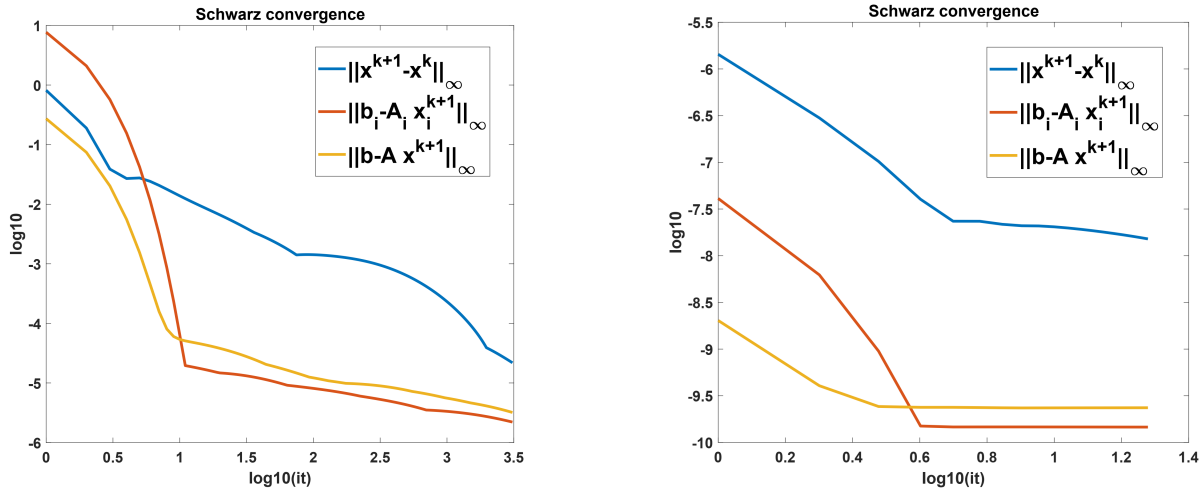

(a) $x^{(0)} = 0$. (b) SVD solution of $Ax^{(0)} = b$.

Figure 3: Convergence of the Schwarz DDM on 8 partitions with respect to the iterations for two initial guesses for the monopole scattered by a rigid sphere with $N_s = 3{,}200, N = 6{,}400, k = 400\,\text{Hz}, \epsilon = 10^{-12}, \tau = 0.8$.

Table 2 exhibits the conditioning number for $\bar{A}_i$ for the sphere problem. They are up to ten orders lower than for the original full system.

Figure 3 shows the convergence behavior of the projected Schwarz algorithm with respect to the iterations. It exhibits a fast convergence starting from the arbitrary initial guess $x^{(0)} = 0$ followed by a slow convergence, see Fig. 3a, and an improvement on the solution starting from the initial guess solution of $Ax^{(0)} = b$ computed by SVD , see Fig. 3b. Let us notice that the algorithm is still stable after the convergence.

The talk will also focus on the numerical and parallel performances of the proposed projected Schwarz algorithm on larger size problems using the PETSc and SLEPc libraries for the implementation.

References

[1] S. Lee, Review: The Use of Equivalent Source Method in Computational Acoustics, Journal of Computational Acoustics 25 (1) (Mar 2017). doi:10.1142/S0218396X16300012.

[2] J. Chambon, T. Le Magueresse, O. Minck, J. Antoni, Three-dimensional beamforming for wind tunnel applications using ESM based transfer functions, in: Proceedings on CD of the 8th Berlin Beamforming Conference, 2-3 March, 2020, 2020.
URL https://www.bebec.eu/fileadmin/bebec/downloads/bebec-2020/papers/BeBeC-2020-S09.pdf

[3] J. Chambon, J. Antoni, S. Bouley, Galerkin equivalent sources method for sound field reconstruction around diffracting bodies, J. Acoust. Soc. Am. 152 (4) (2022) 2042–2053. doi:10.1121/10.0014422.

[4] Y. Bobrovnitskii, T. Tomilina, General-Properties and Fundamental Errors of the Method of Equivalent Sources, Acoustical Physics 41 (5) (1995) 649–660.

[5] L. Berenguer, D. Tromeur-Dervout, Sparse Aitken–Schwarz domain decomposition with application to Darcy flow, Computers & Fluids 249 (2022) 105687. doi:10.1016/j.compfluid.2022.105687.